

A Journal of the Gesellschaft Deutscher Chemiker

Angewandte Chemie

GDCh

International Edition

www.angewandte.org

Accepted Article

Title: Transformation pathway from CdSe magic-size clusters with absorption doublets at 373/393 nm to clusters at 434/460 nm

Authors: Jinming Zhu, Zhaopeng Cao, Yongcheng Zhu, Nelson Rowell, Yan Li, Shanling Wang, Chunchun Zhang, Gang Jiang, Meng Zhang, Jianrong Zeng, and Kui Yu

This manuscript has been accepted after peer review and appears as an Accepted Article online prior to editing, proofing, and formal publication of the final Version of Record (VoR). This work is currently citable by using the Digital Object Identifier (DOI) given below. The VoR will be published online in Early View as soon as possible and may be different to this Accepted Article as a result of editing. Readers should obtain the VoR from the journal website shown below when it is published to ensure accuracy of information. The authors are responsible for the content of this Accepted Article.

To be cited as: *Angew. Chem. Int. Ed.* 10.1002/anie.202104986

Link to VoR: <https://doi.org/10.1002/anie.202104986>

RESEARCH ARTICLE

Transformation pathway from CdSe magic-size clusters with absorption doublets at 373/393 nm to clusters at 434/460 nm

Jinming Zhu⁺, Zhaopeng Cao⁺, Yongcheng Zhu, Nelson Rowell, Yan Li, Shanling Wang, Chunchun Zhang, Gang Jiang, Meng Zhang,^{*} Jianrong Zeng^{*} and Kui Yu^{*}

[*] Jinming, Zhu, Yongcheng, Zhu, Gang, Jiang, Meng, Zhang, Kui, Yu
Institute of Atomic and Molecular Physics, Sichuan University
Chengdu, Sichuan, 610065 (P. R. China)
E-mail: mengzhang@scu.edu.cn
kuiyu@scu.edu.cn
Zhaopeng, Cao, Yan, Li, Jianrong, Zeng
Shanghai Institute of Applied Physics, Chinese Academy of Sciences
Shanghai, 201800 (P. R. China)
E-mail: zengjianrong@sinap.ac.cn
Zhaopeng, Cao, Yan, Li
School of Physical Science and Technology, ShanghaiTech University
Shanghai, 201210 (P. R. China)
Zhaopeng, Cao, Yan, Li
University of Chinese Academy of Sciences
Beijing, 100049 (P. R. China)

Nelson Rowell
Metrology Research Centre, National Research Council Canada
Ottawa, Ontario K1A 0R6 (Canada)
Shanling, Wang, Chunchun, Zhang
Analytical & Testing Center, Sichuan University
Chengdu, Sichuan, 610065 (P. R. China)
Jianrong, Zeng
Shanghai Synchrotron Radiation Facility, Shanghai Advanced
Research Institute, Chinese Academy of Sciences
Shanghai, 201204 (P. R. China)
Kui, Yu
Engineering Research Center in Biomaterials, Sichuan University
Institution
Chengdu, Sichuan, 610065 (P. R. China)

[*] These authors contributed equally to this work.

Supporting information for this article is given via a link at the end of the document.

Abstract: Divergent interpretations have appeared in the literature regarding the structural nature and evolutionary behavior for photoluminescent CdSe nano-species with sharp doublets in optical absorption. Here, we report a comprehensive description of the transformation pathway from one CdSe nano-species displaying an absorption doublet at 373/393 nm to another species with a doublet at 433/460 nm. These two nano-species are shown to be as zero-dimension (0D) magic-size clusters (MSCs) with 3D quantum confinement, and are labelled dMSC-393 and dMSC-460, respectively. Synchrotron-based small angle X-ray scattering (SAXS) returns a radius of gyration of 0.92 nm for dMSC-393 and 1.14 nm for dMSC-460, and indicates that both types are disc-shaped with the exponent of the SAXS form factor equal to 2.1. The MSCs develop from their unique counterpart precursor compounds (PCs), which are labelled PC-393 and PC-460, respectively. For the dMSC-393 to dMSC-460 transformation, the proposed PC-enabled pathway is comprised of three key steps, dMSC-393 to PC-393 (Step 1), PC-393 to PC-460 (Step 2 involving monomer addition), and PC-460 to dMSC-460 (Step 3). The present study provides a framework for understanding the PC-based evolution of MSCs and how PCs enable transformations between MSCs.

Introduction

It has been shown that magic-size clusters (MSCs) have their own unique precursor compounds (PCs).^[1,2] This concept has recently been demonstrated in the synthesis of various II-VI metal chalcogenide (ME) MSCs, which include CdS,^[3-7] CdSe,^[8,16] CdTe,^[9-12,17] CdTeSe,^[13,14] and ZnSe.^[15] In all these cases binary PCs start to form before conventional binary ME quantum dots (QDs) nucleate and grow. This pre-nucleation stage is also known as the QD induction period. The growth relationship between the binary ME MSCs and corresponding QDs can be adequately elucidated with a recently developed two-pathway model.^[1,2] The pathway from MSCs to QDs in this model is similar to that previously proposed in which the MSCs provide a reservoir of monomers for the QDs,^[18]

and includes an additional step in which MSCs transform into monomers via PCs (Scheme S1).

While MSCs exhibit characteristic optical absorption at specific wavelengths, their counterpart PCs do not absorb at these or longer wavelengths.^[1-17] Here the MSCs and their PCs exist as quasi isomers, which can reversibly interchange via intramolecular reorganization. Furthermore, some transformations display isosbestic points, such as between CdS MSC-311 and 322,^[7] among CdTe MSC-371, 417, and 448,^[10-12] and between binary CdTe MSC-371 and ternary CdTeSe MSC-399.^[14] The numbers represent the peak positions in wavelength (nanometers (nm)) of the sharp optical absorption singlets of the MSCs. Following the concept that the MSCs evolve from their own unique PCs, the pathway for these apparent transformations between two types of MSCs has been hypothesized to be PC-enabled, with substitution reactions of monomers that transform the reactant MSC PC into the product MSC PC (Figure S1a).^[1,7,8,10-12,14]

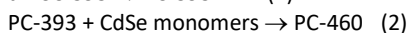
In addition to the MSCs that display sharp optical absorption singlets,^[3-15,18-26] there is another type of nano-species that exhibits sharp optical absorption doublets.^[16,17,27-44] An example semiconductor is photoluminescent (PL) CdSe peaking at around 373/393 (Species-393) or 433/460 nm (Species-460).^[16,27-30] Different assignments have been made,^[35-39] with 0-dimension (0D) dMSC-393 and/or 2D nanoplates NPL-393 for Species-393, and dMSC-460 and/or NPL-460 for Species-460. Meanwhile, the dMSCs (such as dMSC-460 with 3D quantum confinement) and their corresponding NPLs (such as NPL-460 with 1D quantum confinement) exhibit different polarized photoluminescence (PL) but with similar optical absorption.^[16,38,39]

As shown by Figure S1b, the NPLs appear to be comprised of n layers of Cd and $n - 1$ layers of Se.^[40,41] In this scheme, three layers of Cd and two layers of Se make up NPL-393, while four layers of Cd and three layers of Se form NPL-460. Thus, NPL-393 has one fewer CdSe monolayer (ML) than NPL-460. Various formation schemes have been proposed for these NPLs, including the self-assembly of 0D dMSC-460 to 2D NPL-460 (Figure S1c).^[38,42-44] For reaction

RESEARCH ARTICLE

mixtures of various Cd and Se precursors, the evolution of both Species-393 and Species-460 has been reported, with a decrease of the former and an increase of the latter at relatively late points in the reaction (Figure S1d).^[16,27-30] Although there were indications that dMSC-393 and dMSC-460 formed from transformations of their respective counterpart PC-393 and PC-460,^[16] the present study provides the first exposition of their growth relationship.

Here we report our exploration of the pathway for the transformation from PL CdSe dMSC-393 to dMSC-460. Based on what we have seen in our experiments, we propose that the PC-enabled pathway as illustrated in Scheme 1 is responsible for the transformation from smaller dMSC-393 to larger dMSC-460; the two types of PL CdSe dMSCs are disc-shaped. The three key steps labelled in Scheme 1 can be represented by three equations, which are



Steps 1/4 and Steps 3'/3 represent the reversible transformations between dMSC-393 and PC-393 and between dMSC-460 and PC-460, respectively. Step 2 denotes the PC-393 to PC-460 transformation, which occurs as a result of the addition reaction of monomers. Thus, this PC-enabled pathway is different from that proposed before with the substitution reaction of monomers,^[1,7,8,10-12,14] and can also account for the addition of a CdSe monolayer on one of four identical facets of a tetrahedrally-

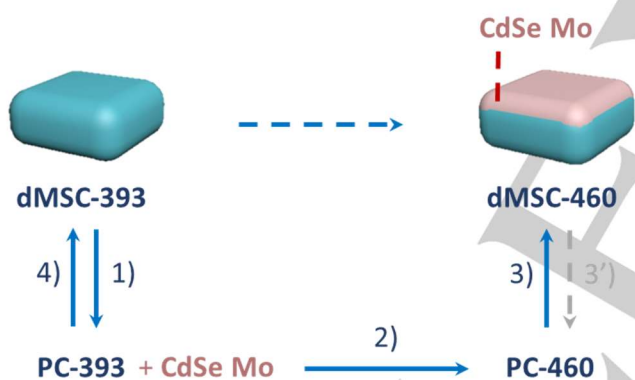
shaped CdSe cluster.^[24] Notably, the monomer addition takes place on PC-393 (Step 2, Equation 2), instead of on dMSC-393 directly. The present understanding on the PC-enabled pathway (Scheme 1) provides a more comprehensive explanation for a number of phenomena. These include the direct evolution of dMSC-460 during a reaction without the presence of dMSC-393 (Part A of Figure S1d),^[27] the formation of NPLs (Figure S1c),^[38,42-44] and the transformation from one type of NPLs to the next thicker NPLs with an additional ME monolayer (Part B of Figure S1c and Scheme S2).^[43] A common assumption for the growth is the direct addition of monomers, but our study (Scheme 1) does not support this assumption.

Results and Discussion

This section is primarily comprised of two parts. The first part addresses optical absorption and PL (with excitation wavelength of 350 nm) properties (Figures 1-3), and the second part deals with synchrotron-based small angle X-ray scattering (SAXS) (Figure 4). Reactions of cadmium myristate Cd(MA)₂ and Se were carried out in 1-octadecene (ODE), with acetic acid (HOAc) added at 110 °C when the reaction was in the induction period occurring prior to nucleation and growth of CdSe QDs. The effect of HOAc addition in the induction period has been reported elsewhere.^[16,38] When the reaction temperature was kept at 190 °C for a period of 5 min, Sample A (light yellow in color) was obtained, while Sample B (deep yellow in color) came from the reaction at 230 °C for 30 min. The two samples, purified by toluene (Tol), contained mainly dMSC-393 (white) and dMSC-460 (deep yellow), respectively.

dMSC-393 (purified Sample A) was heated directly (without dilution in ODE) (Figure 1) and in ODE (Figure 2), with a similar heating procedure which was employed also for the reaction of Cd(MA)₂ and Se in ODE with HOAc added at 110 °C (Figure 3). While the dMSC-393 to dMSC-460 transformation occurred at the lower temperature of 210 °C, an evolution of dMSC-460 was the principal process observed at 230 °C (Figure 1, Parts a and b of Figure 2, and Part a of Figure 3). An almost featureless optical absorption around 210 °C was observed for purified Sample A (Figures 1 and 2), but not for the two reaction mixtures of Cd(MA)₂ and Se (Figure 3). This result can be explained as PC-393 and CdSe monomers (Scheme 1) being generated differently in purified Sample A (Figures 1 and 2) and in the reaction mixtures (Figure 3). Synchrotron-based small angle X-ray scattering (SAXS) delivers the morphological information that dMSC-393 and dMSC-460 have the exponent of the SAXS form factor close to 2, together with the respective radius of gyration (R_g) of 0.92 and 1.14 nm (Figure 4). In this regard, they are disc-shaped and not spherical, and dMSC-393 (Sample A) is smaller than dMSC-460 (Sample B). The SAXS form factor (within the high- q region) has a power law behavior, where the exponent is the signature of the shape of the object. The value of the exponent varies from 0 to 4, with 1.0 for long rods, 2.0 for discs, and 4.0 for smooth-surface spheres.^[45] On the basis of the experimental observations, we propose that the dMSC-393 to dMSC-460 transformation is PC-enabled (Scheme 1).

In Figure 1 we present the evolution of optical absorption and PL properties for purified Sample A at various temperatures. This purified sample was almost white in color at room temperature, and Figure S1-1 shows the optical properties of Sample A (as-synthesized and purified), with corresponding TEM and XRD results shown in Figure S1-2. It is evident that Sample A (after purification with Tol) still contained mostly OD dMSC-393. When dMSC-393



Scheme 1. Schematic drawing of the proposed pathway for the PC-enabled transformation from dMSC-393 to dMSC-460. The pathway involves three sequential steps, which are isomerization from dMSC-393 to PC-393 (Step 1 Eq 1), the reaction with CdSe monomer (Mo) addition that transforms PC-393 into PC-460 (Step 2 Eq 2), and isomerization from PC-460 to dMSC-460 (Step 3 Eq 3). When dMSC-393 (contained in purified Sample A by toluene) was heated (Figures 1 and 2), Step 1 occurred, and monomers were then generated from the fragmentation of PC-393 and Step 2 took place. In the reaction of Cd(MA)₂ and Se in ODE (Figure 3), dMSC-393 and dMSC-460 preferred relatively high and low Se feed concentrations, respectively; this can be explained by the competition between Steps 4 and 2 due to the direct production of PC-393 and monomers, which is different from that when dMSC-393 was heated (Figures 1 and 2). Synchrotron-based SAXS suggests that dMSC-393 is smaller than dMSC-460, both of which are disc-shaped (Figure 4). The proposed PC-enabled pathway allows for the addition of a CdSe monolayer on one of the four identical facets of a CdSe tetrahedra cluster.^[24]

RESEARCH ARTICLE

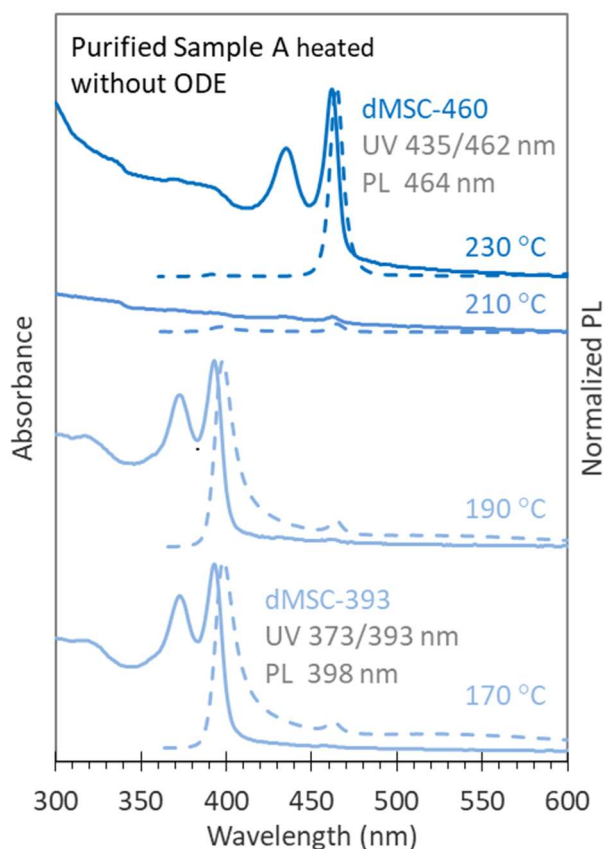


Figure 1. Optical characteristics of the transformation from dMSC-393 to dMSC-460 when dMSC-393 (purified Sample A) was heated (without ODE). Sample A was obtained from a reaction (190 °C/5 min) of Cd(MA)₂ and Se in ODE, with the addition of HOAc within the induction period (110 °C). Sample A was purified three times with Tol, and the resulting precipitate (dMSC-393 about 50 mg) was heated directly. From 170 to 230 °C (in temperature steps of 20 °C with a 5 min hold time at each step), four samples were extracted and dispersed in Tol for the measurements of optical absorption (left y axis, solid traces) and PL (right y axis, dashed traces normalized) (offset). At 210 °C, dMSC-393 almost disappeared from the spectrum, whereas dMSC-460 increased in strength from 210 to 230 °C. Remarkably, Sample A displayed almost featureless optical properties at 210 °C, which supports the PC-enabled pathway as depicted by Scheme 1 for the apparent transformation from dMSC-393 to dMSC-460.

(purified Sample A) was heated directly without using ODE, four samples were taken from 170 to 230 °C (in temperature steps of 20 °C after 5 min at each step). Each extracted sample was dispersed in 3.0 mL Tol for the optical absorption and PL measurements.

When dMSC-393 (purified Sample A) was heated at 170 and 190 °C, dMSC-393 remained, exhibiting an optical absorption doublet peaking at ~373/393 nm and a PL peak at ~398 nm. At 210 °C, this sample transitioned to display a relatively featureless absorption, compared to the other three temperatures. Thus, it is evident that the dMSC-393 to PC-393 transformation was more or less complete at this temperature (Scheme 1 Step 1). While Scheme 1 describes our understanding of the transformation process, any reference to a specific step in the following discussion refers to Scheme 1 utterly, such as Step 1. At 230 °C, a new absorption doublet appeared in the spectrum at 435/462 nm with the corresponding PL peaking at 464 nm, which indicates the development of dMSC-460 (from PC-460, Step 3). Accordingly, Sample A contained dMSC-393 from room temperature to 190 °C, but dMSC-460 at 230 °C. The

absorption and emission spectra for the two species have similar full width at half maximum (FWHM) of ~10 nm. Furthermore, we noticed that purified Sample A was quite viscous even at 210 °C with very light yellow color. At 230 °C, it became deep yellow with its viscosity decreased a little. It is reasonable that a sample containing dMSC-393 would be light yellow in color, while one containing dMSC-460 would be deep yellow, consistent with a size increase from the former to the latter.

Therefore, a dMSC-393 to dMSC-460 transformation around 210 °C is indicated by both the color change and the featureless absorption spectrum at that temperature. At approximately this critical temperature, purified Sample A contained a barely detectable concentration of dMSC-393, and a small amount of dMSC-460. We therefore propose that at this stage, dMSC-393 transforms to its PC-393 (Step 1), followed by the transformations from PC-393 to PC-460 (Step 2) and to dMSC-460 (Step 3). The PC-460 to dMSC-460 transformation (Step 3) is apparently more efficient at higher temperatures such as 230 °C.

For the PC-393 to PC-460 transformation (Step 2), we expected that it is affected by the amount of dMSC-393. Thus, we diluted dMSC-393 by ODE. In Figure 2 we present the evolution of optical absorption and PL for dMSC-393 diluted in ODE and subjected to a similar thermal processing to that for Figure 1. The concentrations of purified Sample A (identical to that used for Figure 1) in ODE were 10.0 (a), 5.0 (b) and 2.5 mg·mL⁻¹ (c), which are smaller than that in Figure 1. From 150 to 250 °C (with temperature steps of 20 °C and 5 min at each step), six samples were taken. For the optical measurements, a volume of 50 (a), 50 (b), and 200 μL (c) of each extracted sample was dispersed in 3.0 mL of Tol.

The optical properties of dMSC-393 (purified Sample A) in ODE shown in Parts a and b of Figure 2 evolved in a similar fashion to that shown in Figure 1. When the concentration of Sample A was as high as 10.0 mg·mL⁻¹ (Part a), dMSC-393 increased in strength from 150 to 170 °C, and then decreased from 170 to 210 °C. It is reasonable that the increase is due to more dMSC-393 being dissolved at 170 °C than at 150 °C. At 210 °C, Sample A displayed relatively featureless optical absorption and PL spectra, as compared to at the other five temperatures. From 210 to 250 °C, dMSC-460 increased in strength. When the concentration of Sample A was 5.0 mg·mL⁻¹ (Part b), dMSC-393 decreased in strength from 150 to 210 °C. This purified sample displayed relatively featureless optical absorption and PL spectra at 210 °C. From 230 to 250 °C, dMSC-460 increased in strength. When the concentration of Sample A was as low as 2.5 mg·mL⁻¹ (Part c), dMSC-393 decreased in strength from 150 to 190 °C. From 190 to 230 °C, Sample A had relatively featureless optical absorption and PL spectra. At 250 °C, a broad absorption peaking at ~607 nm emerged, which indicates the presence of CdSe QDs.

The optical properties of Sample A in the three batches for Figure 2 became different mainly after 190 °C. The optical properties have been compared for the stages from 150 to 170 °C (Figure S2-1), from 190 to 210 °C (Figure S2-2), and from 230 to 250 °C (Figure S2-3). The lower the concentration was, the broader the temperature window was for featureless optical absorption, such as at 210 °C (Figures 1 and 2a), from 210 to 230 °C (Figure 2b), and from 190 to 230 °C (Figure 2c). The temperature ranges with featureless optical absorption are symptomatic of complete dMSC-393 to PC-393 transformation (Step 1). When the concentration of dMSC-393 was relatively high (such as shown in Figure 1 and Part a of Figure 2), the dMSC-393 to dMSC-460 transformation appeared to dominate. When the concentration was relatively low (Figure 2 Part

RESEARCH ARTICLE

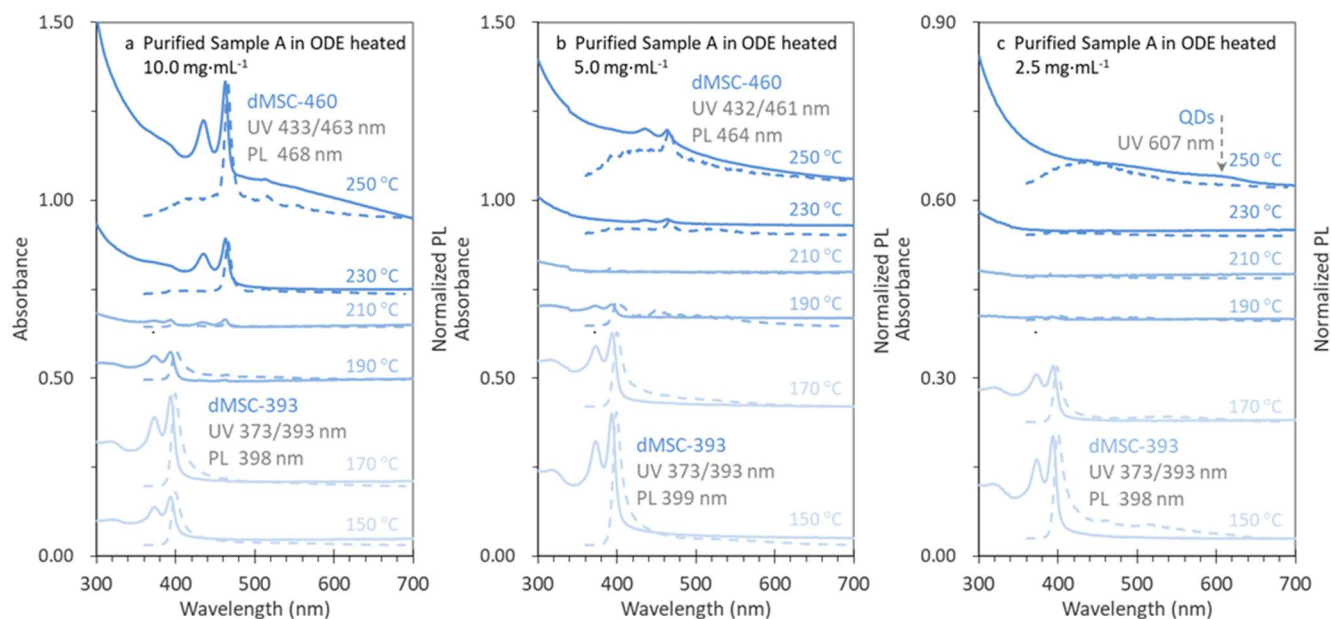


Figure 2. Optical absorption (solid traces) and PL (dashed traces, normalized) spectra when dMSC-393 (purified Sample A) was heated in ODE with concentrations of 10.0 (a), 5.0 (b) and 2.5 (c) mg·mL⁻¹. For each batch, six samples were extracted between 150 and 250 °C (using a similar procedure to that used for Figure 1). For the optical measurements, 50 μ L (a and b) or 200 μ L (c) of each sample was dispersed in 3.0 mL of Tol. During the temperature increase, the signal for dMSC-393 disappeared at 210 °C (a and b, similar to Figure 1) or at 190 °C (c). For the largest concentration (a), dMSC-460 started to evolve at 210 °C (similar to the behavior in Figure 1). For the medium concentration (b), dMSC-460 appeared at 230 °C. For the lowest concentration (c), QDs nucleated and grew at temperatures above 230 °C. A featureless optical absorption was observed at 210 °C (a and b) or between 190 and 210 °C (c). At sufficiently high concentrations (a and b), the fragmentation of PC-393 enabled the dMSC-393 to dMSC-460 transformation (Scheme 1). At low concentrations (c), the fragmentation of PC-393 facilitated the nucleation and growth of conventional QDs (Scheme S1).^[1,2]

c), the dMSC-393 to QD transformation occurred readily. We therefore propose that during the increase of the temperature, dMSC-393 transferred to PC-393 below 210 °C (via Step 1). At sufficiently high concentrations (Parts a and b in Figure 2 as well as Figure 1), some PC-393 fragmented into monomers, which transformed the remaining PC-393 to PC-460 at \sim 210 °C (via Step 2). Thus, dMSC-460 evolved (via Step 3). When the concentration of dMSC-393 was low (Part c in Figure 2), almost all PC-393 fragmented, feeding the nucleation and growth of QDs observed at temperatures higher than 230 °C. The MSC to PC to monomer to QD pathway (as shown in Scheme S1) has been illustrated elsewhere.^[1-3]

To assess the hypothesis of the PC-enabled transformation shown in Scheme 1, we carried out reactions using a 4Cd to 1Se feed molar ratio with eight Se feed concentrations ranging from 1.9 to 75.0 mmol·kg⁻¹ as shown in Figures 3 and S3-1. For the study in which we started with dMSC-393 (purified Sample A as presented in Figures 1 and 2), PC-393 was generated as a result of heating (as described by Step 1), which caused monomers to be produced via the fragmentation of PC-393. However, for reaction mixtures of Cd(MA)₂ and Se in ODE (with the addition of HOAc in the induction period at 120 °C),^[16,38] PC-393 and monomers will form prior to dMSC-393.^[16,38] In this case, the PC-393 to dMSC-393 transformation (Step 4) competes with the PC-393 to PC-460 transformation (Step 2). The relative evolution of dMSC-393 and dMSC-460 is expected to be different for reaction mixtures of Cd(MA)₂ and Se (Figures 3 and S3-1), compared to that for dMSC-393 (purified Sample A shown in Figures 1 and 2).

In Figure 3 we present the evolution of the optical properties of samples extracted from two reaction mixtures of Cd(MA)₂ and Se in ODE with the Se concentrations of 37.5 (a) and 7.5 (b) mmol·kg⁻¹

1. The addition of HOAc was performed at 110 °C. From 170 to 250 °C in 20 °C steps, six samples were taken. For the optical measurements, a volume of 10 μ L (Batch a) or 50 μ L (Batch b) from each extracted sample was dispersed in 3.0 mL of Tol. For the reaction mixture with a relatively high Se concentration of 37.5 mmol·kg⁻¹ (Part a of Figure 3), dMSC-393 seemed to evolve at 170 °C and increased in strength at 210 °C. At 230 °C, dMSC-393 decreased, while dMSC-460 developed. At 250 °C, dMSC-393 disappeared completely (according to PL), while dMSC-460 increased in strength. The coexistence of dMSC-393 and dMSC-460 at 230 °C is noteworthy, and the evolution of dMSC-460 seems to be at the expense of dMSC-393. This effect has also been observed in the reaction mixture of cadmium stearate (Cd(St)₂) and Se (Figure S3-2). For the reaction mixture with a relatively low Se concentration of 7.5 mmol·kg⁻¹ (Part b of Figure 3), dMSC-393 did not appear to evolve, while dMSC-460 did at a relatively low temperature of 190 °C. Afterwards, dMSC-460 kept increasing in strength (up to the maximum monitored temperature of 250 °C). The evolution of dMSC-460 without dMSC-393 in Batch b is noteworthy; the absence of dMSC-393 is consistent with the concept that dMSC-460 directly transforms from PC-460 (Step 3 of Scheme 1) and not from dMSC-393.

The PC-enabled transformation pathway depicted in Scheme 1 provides a basic understanding of the various relationships observed for the evolution of dMSC-393 and dMSC-460 in the reaction mixtures shown in Figures 3 and S3-1. We argue that for the reaction mixture of Figure 3 Batch a, the direct formation of PC-393 and the PC-393 to dMSC-393 transformation (Step 4) both started around 170 °C. At 230 °C, the PC-393 to PC-460 transformation (Step 2) and PC-460 to dMSC-460 transformation (Step 3) took over. For the reaction mixture of Figure 3 Batch b, Step

RESEARCH ARTICLE

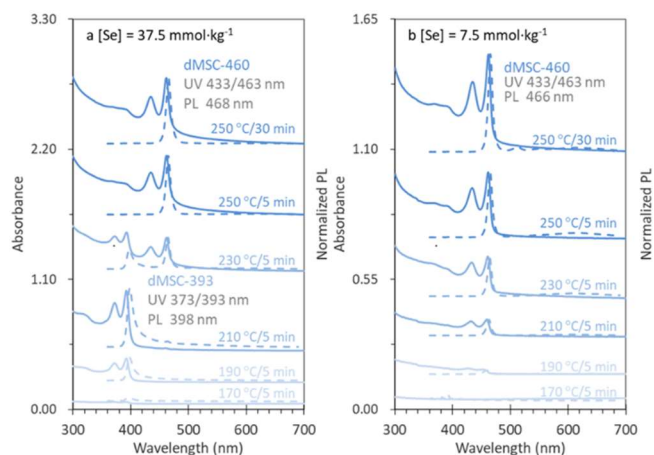


Figure 3. Evolution of optical absorption (solid traces) and PL (dashed traces, normalized) spectra for samples from two reactions with Se feed concentrations of 37.5 (a) and 7.5 (b) mmol·kg⁻¹. The reactions in ODE had a feed molar ratio of 4Cd(MA)₂ to 1Se, with the HOAc addition at 110 °C prior to the nucleation and growth of QDs. Six samples were extracted from 170 to 250 °C as indicated. For the optical measurements, a volume of 10 (a) and 50 (b) μL of each sample was dispersed in 3.0 mL of Tol. For Batch a, dMSC-393 evolved at 170 °C and increased at 210 °C, while dMSC-460 evolved at 230 °C and increased at 250 °C. For Batch b, only dMSC-460 evolved at 190 °C and increased at 250 °C. The evolution of dMSC-393 competed with that of dMSC-460 for Batch a, while dMSC-460 evolved with the absence of dMSC-393 for Batch b. With the PC-enabled transformation pathway (Scheme 1) providing a basic understanding of the experimental observations, it is reasonable that the Se feed concentration affects the evolution relationships. The lower the Se feed concentration, the smaller the amount of PC-393 produced. Relatively large and small amounts of PC-393 favor Steps 4 and 2, respectively; hence, relatively high and low Se feed concentrations facilitate the evolution of dMSC-393 and dMSC-460, respectively.

4 was inhibited due to a low concentration of PC-393, while Step 2 occurred at a relatively low temperature of 190 °C, together with Step 3. From 190 °C to higher temperatures (such as 250 °C), Steps 2 and 3 continued and dMSC-460 increased in strength.

Thus, for the reaction mixtures of Cd(MA)₂ and Se in ODE, the development of dMSC-393 from PC-393 via Step 4 competes with that of dMSC-460 via Steps 2 and 3. This competition (between Steps 4 and 2) can be tuned by the Se feed concentration, which strongly influences the amount of PC-393. For example (Figures S3 and S3-1), when the Se feed concentration was 37.5, 30.0, and 15.0 mmol·kg⁻¹, both dMSC-393 and dMSC-460 were observed at 230, 210, and 190 °C, respectively. Figure S3-3 shows the optical properties of the samples extracted at 210 °C from the eight batches shown in Figures 3 and S3-1. When the Se concentration was decreased to 7.5 and 3.8 mmol·kg⁻¹, dMSC-460 started to evolve at 190 °C without dMSC-393 being present. Thus, Step 4 is favored by a relatively high Se feed concentration (such as above 15.0 mmol·kg⁻¹), while Step 2 by a relatively low Se feed concentration (such as 7.5 mmol·kg⁻¹).

Furthermore, the reaction mixtures (shown in Figures 3 and S3-1) did not have a temperature interval of featureless optical absorption, such as that observed for purified Sample A (as shown in Figures 1 and 2) between 190 and 210 °C. We attribute this difference to the different generation of PC-393 and monomers, which are direct in the reaction mixtures (before dMSC-393 could form) and indirect in purified Sample A (via Step 1 and the fragmentation of PC-393, respectively). With both monomers and

PC-393 present in the reaction mixtures, the PC-393 to PC-460 transformation (Step 2) was relatively likely. Subsequently, a continuous increase of dMSC-460 was observed with increasing temperature (in the presence or absence of dMSC-393 depending on the Se feed concentration).

To examine further our hypothesis of the PC-enabled transformation shown in Scheme 1, we carried out also synchrotron-based SAXS. With excellent statistics as well as simple and non-damaging sample preparation, SAXS has been applied to investigate various semiconductor nanostructures, including QDs,^[46-48] MSCs,^[9,13,19] and NPLs.^[49,50] Part a of Figure 4 presents the SAXS profiles collected from purified Samples A (blue circular symbols) and B (red square symbols) at room temperature. Three Bragg peaks are observed for both purified samples. Also, Part a contains the corresponding traces for the data fitted assuming two unified Guinier-Porod levels (Level 1 (L1) and Level 2 (L2)) and three Lorentz peaks. See Experimental methods in Supplementary Information for the method used for the data fitting. The fitted SAXS data (the vertical values of Part a) are mathematically separated and presented in Parts b and c of Figure 4, with blue for purified Sample A and red for purified Sample B. Part b (the form factor) shows the L1 and L2 signals, and Part c (the structure factor) the three Lorentz peak signals. The scale of the y axis of Part b is about 100 times larger than that of Part c.

The SAXS result shown in Part a is consistent with the TEM and

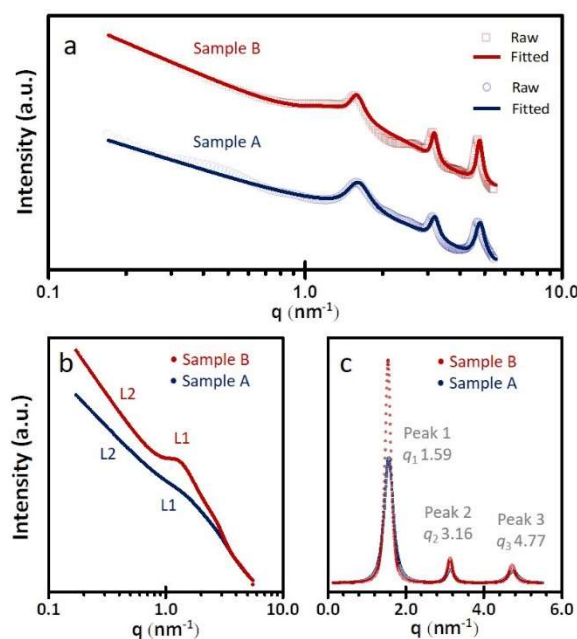


Figure 4. SAXS investigation of dMSC-393 (purified Sample A) and dMSC-460 (purified Sample B). The two samples were kept for 7 days before the measurements. Part a contains the original SAXS profiles which were collected at room temperature, with blue circles for Sample A and red squares for Sample B. The blue and red traces in Part a represent the corresponding fitted data which are separated presented in Parts b and c as well. In Part b, the scattering signals Level 1 (L1) suggest that dMSC-393 and dMSC-460 are disc-shaped and have the respective radii of gyration (R_g) of 0.92 and 1.14 nm. The scattering signals Level 2 (L2) indicate that dMSC-393 and dMSC-460 aggregated.^[9] In Part c, the three Lorentz peaks, q_1 , q_2 , and q_3 , have the peak position ratio of 1 : 2 : 3, signifying the presence of multilayered nanostructures in both samples with the same layered spacing of $2\pi/q_1$.^[49,51]

RESEARCH ARTICLE

XRD study shown in Parts a and b of Figures S1-2 and S4-2 for Samples A and B purified with Tol, respectively. We note that purified Sample A used for Figures 1, 2, and 4 was from the same synthetic batch. In the same presentation format as Figures S1-1 and S1-2 for Sample A, Figure S4-1 shows the optical properties of Sample B (as-synthesized and purified). The corresponding TEM and XRD results are shown in Figure S4-2. Combined with the TEM and XRD results, we attribute the two types of scattering signals shown in Parts b and c to OD and 2D species, respectively. Each of the two samples contained a mixture of OD and 2D species, with the latter species in a relatively small amount. See Scheme S2 for the possible connection between these species.

The OD species related scattering signals shown in Part b suggest that dMSC-393 and dMSC-460 respectively have the radius of gyration (R_g) of 0.92 and 1.14 nm, and they have a similar exponent of the SAXS form factor of 2.1. Thus, dMSC-393 is smaller than dMSC-460, both of which are disc-shaped. See Figure S4-3 for our size estimation for dMSC-393 and dMSC-460. The effect of Cd to Se feed molar ratios on the evolution of dMSC-393 and dMSC-460 (Figures S4-4 and S4-5) shows that relatively high and low Cd to Se feed molar ratios favor dMSC-393 and dMSC-460, respectively. This is in agreement with the SAXS result that dMSC-393 is smaller than dMSC-460.

For the 2D species related scattering signals shown in Part b, these two sets of peaks appear at the same positions of 1.59 (q_1), 3.16 (q_2), and 4.77 nm⁻¹ (q_3). The apparent ratios of the peak positions of q_1 to q_2 to q_3 are about 1 to 2 to 3. Such a result suggests the presence of layered structures in both samples. The two layered structures have a similar interlayered spacing, which is estimated to be about 3.95 nm from the calculation of $2\pi/q_1$.^[49,51] See Figure S4-6 for further explanation. It is necessary to point out that purified Samples A and B were kept for 7 days before performing the SAXS measurements; thus, the self-assembly of dMSC-393 and dMSC-460 had proceeded during the storage period to a certain degree,^[16] with the majority of the OD dMSCs remaining.

Conclusion

We have proposed a PC-enabled pathway (as depicted in Scheme 1) that is responsible for the transformation from one PL CdSe species to another, based on the present experimental data and data analysis. The two species display sharp optical absorption doublets at 373/393 and 433/463 nm, with PL peaking around 399 and 466 nm, respectively. We performed reactions of Cd(MA)₂ and Se in ODE, with HOAc addition in the induction period at 110 °C prior to nucleation and growth of CdSe QDs. Two samples, A and B, were obtained respectively at 190 and 230 °C. After being purified with Tol, the two samples still respectively contained mainly OD dMSC-393 and OD dMSC-460, as suggested by TEM, XRD, and synchrotron-based SAXS. Furthermore, SAXS indicated that the radius of gyration (R_g) was 0.92 and 1.14 nm for dMSC-393 and dMSC-460, respectively, and they were disc-shaped with the exponent of the SAXS form factor close to 2 (Figure 4). Thus, dMSC-393 is smaller than dMSC-460, and they can be selectively synthesized with relatively high and low Cd to Se feed molar ratios. With the monomer addition (Step 2) that allows smaller dMSC-393 to transform into larger dMSC-460, the PC-enabled pathway (Scheme 1) provides a unique framework that satisfactorily elucidates various experimental observations. When dMSC-393 (purified Sample A) was heated, the dMSC-393 to PC-393

transformation (Step 1) resulted in nearly featureless optical properties at 210 °C (Figures 1 and 2). When the concentration of dMSC-393 was high enough (Figure 1 and Parts a and b of Figure 2), the fragmentation of PC-393 to monomers accounted for the subsequent evolution of dMSC-460 (via Steps 2 and 3). On the other hand, when the concentration of dMSC-393 was low enough (Part c of Figure 2), the fragmentation of PC-393 to monomers resulted in the generation of QDs. For reaction mixtures of Cd(MA)₂ and Se in ODE (Figure 3), the evolution of dMSC-393 was competitive to that of dMSC-460 (Batch a with a relatively high Se feed concentration), while the latter developed without the presence of the former (Batch b with a relatively low Se feed concentration). We argue that the Step 4 (PC-393 to dMSC-393 transformation) competes with Steps 2 and 3 (the PC-393 to PC-460 and dMSC-460 transformation). Furthermore, Steps 4 and 2 are respectively facilitated, when the amount of PC-393 is relatively high and low. Thus, relatively high Se feed concentrations favor dMSC-393, while low concentrations give rise to dMSC-460. We have carried out a preliminary density function theory (DFT) study, as shown by Figures S5-1 to S5-3 (which is based on XRD shown in Part b of Figure S1-2), to assist our understanding of the transformation pathway. More sophisticated theoretical models are needed to understand better the thermodynamics and kinetics of the clusters and their PC-enabled formation. It is worth noting that an understanding of these PL nano-species and their formation will aid their potential applications such as in optoelectronic displays and solid-state lighting.^[52-55] We anticipate that the PC-enabled pathway (Scheme 1) has general applicability for transformations such as from PL CdSe dMSC-460 to dMSC-513,^[36] as well as from PL CdTe dMSC-427 to dMSC-495 to dMSC-550 to dMSC-600.^[31] The present findings bring sophisticated insight into the pathway of the MSC evolution and transformation, the latter of which experiences reactions of monomer substitution^[1] or addition that transform two MSC counterpart PCs.

Acknowledgements

K. Y. thanks the National Natural Science Foundation of China (NSFC) 21773162, the Fundamental Research Funds for the Central Universities, the Applied Basic Research Programs of Science and Technology Department of Sichuan Province 2020YJ0326, the State Key Laboratory of Polymer Materials Engineering of Sichuan University respectively for Grant No. sklpme2020-2-09, and the Open Project of Key State Laboratory for Supramolecular Structures and Materials of Jilin University for SKLSSM 2021030. We thank Prof Jianyi Ma for useful discussions on DFT, and the Analytical & Testing Center of Sichuan University for characterization including TEM and XRD.

Keywords: magic-size clusters (MSCs) □ semiconductor quantum dots (QDs) □ cadmium selenide (CdSe) □ transformation pathway □ colloidal

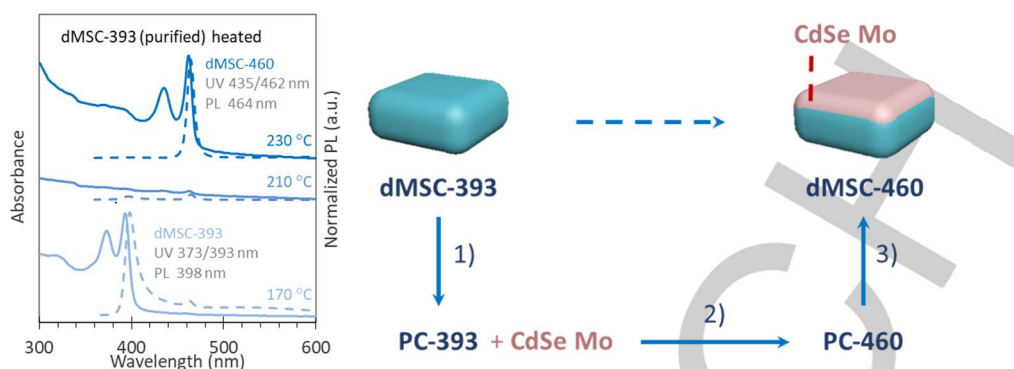
- [1] L. He, C. Luan, N. Rowell, M. Zhang, X. Chen, K. Yu, *Acc. Chem. Res.* **2021**, *54*, 776–786.
- [2] C. Palencia, K. Yu, K. Boldt, *ACS Nano* **2020**, *14*, 1227–1235.
- [3] L. Li, J. Zhang, M. Zhang, N. Rowell, C. Zhang, S. Wang, J. Lu, H. Fan, W. Huang, X. Chen, K. Yu, *Angew. Chem. Int. Ed.* **2020**, *132*, 12111–12119.
- [4] T. Zhu, B. Zhang, J. Zhang, J. Lu, H. Fan, N. Rowell, J. A. Ripmeester, S. Han, K. Yu, *Chem. Mater.* **2017**, *29*, 5727–5735.

RESEARCH ARTICLE

- [5] J. Zhang, X. Hao, N. Rowell, T. Kreouzis, S. Han, H. Fan, C. Zhang, C. Hu, M. Zhang, K. Yu, *J. Phys. Chem. Lett.* **2018**, *9*, 3660–3666.
- [6] W. Wan, M. Zhang, M. Zhao, N. Rowell, C. Zhang, S. Wang, T. Kreouzis, H. Fan, W. Huang, K. Yu, *Nat. Commun.* **2020**, *11*, 4199.
- [7] B. Zhang, T. Zhu, M. Ou, N. Rowell, H. Fan, J. Han, L. Tan, M. T. Dove, Y. Ren, X. Zuo, S. Han, J. Zeng, K. Yu, *Nat. Commun.* **2018**, *9*, 2499.
- [8] D. Zhu, J. Hui, N. Rowell, Y. Liu, Q. Y. Chen, T. Steegemans, H. Fan, M. Zhang, K. Yu, *J. Phys. Chem. Lett.* **2018**, *9*, 2818–2824.
- [9] M. Liu, K. Wang, L. Wang, S. Han, H. Fan, N. Rowell, J. A. Ripmeester, R. Renoud, F. Bian, J. Zeng, K. Yu, *Nat. Commun.* **2017**, *8*, 15467.
- [10] Q. Shen, C. Luan, N. Rowell, M. Zhang, K. Wang, M. Willis, X. Chen, K. Yu, *Inorg. Chem.* **2021**, *60*, 4243–4251.
- [11] C. Luan, Ö. Ö. Gokcinar, N. Rowell, T. Kreouzis, S. Han, M. Zhang, H. Fan, K. Yu, *J. Phys. Chem. Lett.* **2018**, *9*, 5288–5295.
- [12] C. Luan, J. Tang, N. Rowell, M. Zhang, W. Huang, H. Fan, K. Yu, *J. Phys. Chem. Lett.* **2019**, *10*, 4345–4353.
- [13] D. Gao, X. Hao, N. Rowell, T. Kreouzis, D. J. Lockwood, S. Han, H. Fan, H. Zhang, C. Zhang, Y. Jiang, J. Zeng, M. Zhang, K. Yu, *Nat. Commun.* **2019**, *10*, 1674.
- [14] H. Zhang, C. Luan, D. Gao, M. Zhang, N. Rowell, M. Willis, M. Chen, J. Zeng, H. Fan, W. Huang, X. Chen, K. Yu, *Angew. Chem. Int. Ed.* **2020**, *59*, 16943–16952.
- [15] L. Wang, J. Hui, J. Tang, N. Rowell, B. Zhang, T. Zhu, M. Zhang, X. Hao, H. Fan, J. Zeng, S. Han, K. Yu, *Adv. Sci.* **2018**, *5*, 1800632.
- [16] Y. Liu, M. Willis, N. Rowell, W. Luo, H. Fan, S. Han, K. Yu, *J. Phys. Chem. Lett.* **2018**, *9*, 6356–6363.
- [17] M. Chen, C. Luan, M. Zhang, N. Rowell, M. Willis, C. Zhang, S. Wang, X. Zhu, H. Fan, W. Huang, K. Yu, B. Liang, *J. Phys. Chem. Lett.* **2020**, *11*, 2230–2240.
- [18] Z. Jiang, D. F. Kelley, *ACS Nano* **2010**, *4*, 1561–1572.
- [19] D. R. Nevers, C. B. Williamson, B. H. Savitzky, I. Hadar, U. Banin, L. F. Kourkoutis, T. Hanrath, R. D. Robinson, *J. Am. Chem. Soc.* **2018**, *140*, 3652–3662.
- [20] C. B. Williamson, D. R. Nevers, A. Nelson, I. Hadar, U. Banin, T. Hanrath, R. D. Robinson, *Science* **2019**, *363*, 731–735.
- [21] S. Kudera, M. Zanella, C. Giannini, A. Rizzo, Y. Li, G. Gigli, R. Cingolani, G. Ciccarella, W. Spahl, W. J. Parak, L. Manna, *Adv. Mater.* **2007**, *19*, 548–552.
- [22] B. M. Cossairt, J. S. Owen, *Chem. Mater.* **2011**, *23*, 12, 3114–3119.
- [23] Y. Wang, Y. Liu, Y. Zhang, F. Wang, P. J. Kowalski, H. W. Rohrs, R. A. Loomis, M. L. Gross, and W. E. Buhro, *Angew. Chem. Int. Ed.* **2012**, *51*, 6154–6157.
- [24] A. S. Mule, S. Mazzotti, A. A. Rossinelli, M. Aellen, P. T. Prins, J. C. van der Bok, S. F. Solari, Y. M. Glauser, P. V. Kumar, A. Riedinger, D. J. Norris, *J. Am. Chem. Soc.* **2021**, *143*, 2037–2048.
- [25] A. D. Dukes, J. R. McBride, S. J. Rosenthal, *Chem. Mater.* **2010**, *22*, 6402–6408.
- [26] A. Ritchhart, B. M. Cossairt, *Angew. Chem. Int. Ed.* **2018**, *130*, 1926–1930.
- [27] K. Yu, J. Ouyang, M. B. Zaman, D. Johnston, F. J. Yan, G. Li, C. I. Ratcliffe, D. M. Leek, X. Wu, J. Stupak, Z. Jakubek, D. Whitfiel, *J. Phys. Chem. C* **2009**, *113*, 3390–3401.
- [28] F. D. Ott, A. Riedinger, D. R. Ochsenbein, P. N. Knusel, S. C. Erwin, M. Mazzotti, D. J. Norris, *Nano Lett.* **2017**, *17*, 6870–6877.
- [29] Y. Jiang, W. Ojo, B. Mahler, X. Xu, B. Abécassis, B. Dubertret, *ACS Omega* **2018**, *3*, 6199–6205.
- [30] D. A. Kurtina, A. V. Garshev, I. S. Vasil'eva, V. V. Shubin, A. M. Gaskov, R. B. Vasiliev, *Chem. Mater.* **2019**, *31*, 9652–9663.
- [31] R. Wang, J. Ouyang, S. Nikolaus, L. Brestaz, M. B. Zaman, X. Wu, D. Leek, C. I. Ratcliffe, K. Yu, *Chem. Commun.* **2009**, 962–964.
- [32] F. Wang, M. Zhang, W. Chen, S. Javaid, H. Yang, S. Wang, X. Yang, L. Zhang, M. A. Buntine, C. Li, G. Jia, *Nanoscale Adv.* **2020**, *2*, 3316–3322.
- [33] J. Zhang, C. Rowland, Y. Liu, H. Xiong, S. Kwon, E. Shevchenko, R. D. Schaller, V. B. Prakapenka, S. Tkachev, T. Rajh, *J. Am. Chem. Soc.* **2015**, *137*, 742–749.
- [34] D. C. Gary, M. W. Terban, S. J. L. Billinge, B. M. Cossairt, *Chem. Mater.* **2015**, *27*, 1432–1441.
- [35] J. Joo, J. S. Son, S. G. Kwon, J. H. Yu, T. Hyeon, *J. Am. Chem. Soc.* **2006**, *128*, 5632–5633.
- [36] J. Ouyang, M. B. Zaman, F. J. Yan, D. Johnston, G. Li, X. Wu, D. Leek, C. I. Ratcliffe, J. A. Ripmeester, K. Yu, *J. Phys. Chem. C* **2008**, *112*, 13805–13811.
- [37] S. Ithurria, B. Dubertret, *J. Am. Chem. Soc.* **2008**, *130*, 49, 16504–16505.
- [38] Y. Liu, B. Zhang, H. Fan, N. Rowell, M. Willis, X. Zheng, R. Che, S. Han, K. Yu, *Chem. Mater.* **2018**, *30*, 1575–1584.
- [39] Y. Liu, N. Rowell, M. Willis, M. Zhang, S. Wang, H. Fan, W. Huang, X. Chen, K. Yu, *J. Phys. Chem. Lett.* **2019**, *10*, 2794–2801.
- [40] B. Mahler, B. Nadal, C. Bouet, G. Patriarche, B. Dubertret, *J. Am. Chem. Soc.* **2012**, *134*, 18591–18598.
- [41] F. Wang, Y. Wang, Y. Liu, P. J. Morrison, R. A. Loomis, W. E. Buhro, *Acc. Chem. Res.* **2015**, *48*, 13–21.
- [42] S. Ithurria, G. Bousquet, and B. Dubertret, *J. Am. Chem. Soc.* **2011**, *133*, 3070–3077.
- [43] A. Riedinger, F. D. Ott, A. Mule, S. Mazzotti, P. N. Knusel, S. J. P. Kress; F. Prins, S. C. Erwin, D. J. Norris, *Nat. Mater.* **2017**, *16*, 743–748.
- [44] Y. Chen, D. Chen, Z. Li, X. Peng, *J. Am. Chem. Soc.* **2017**, *139*, 10009–10019.
- [45] Y. Ren, X. Zuo, *Small Methods* **2018**, *2*, 1800064.
- [46] B. Abécassis, C. Bouet, C. Garnero, D. Constantin, N. Lequeux, S. Ithurria, B. Dubertret, B. R. Pauw, D. Pontoni, *Nano Lett.* **2015**, *15*, 2620–2626.
- [47] J. Maes, N. Castro, K. De Nolf, W. Walravens, B. Abécassis, Z. Hens, *Chem. Mater.* **2018**, *30*, 3952–3962.
- [48] X. Hao, M. Chen, L. Wang, Z. Cao, Y. Li, S. Han, M. Zhang, K. Yu, J. Zeng, *Chem. Commun.* **2020**, *56*, 2031–2034.
- [49] C. Bouet, B. Mahler, B. Nadal, B. Abécassis, M. D. Tessier, S. Ithurria, X. Xu, B. Dubertret, *Chem. Mater.* **2013**, *25*, 639–645.
- [50] N. Castro, C. Bouet, S. Ithurria, N. Lequeux, D. Constantin, P. Levitz, D. Pontoni, B. Abécassis, *Nano Lett.* **2019**, *19*, 6466–6474.
- [51] Y. H. Liu, F. Wang, Y. Wang, P. C. Gibbons, W. E. Buhro, *J. Am. Chem. Soc.* **2011**, *133*, 17005–17013.
- [52] E. C. Hansen, Y. Liu, H. Utzat, S. N. Bertram, J. C. Grossman, M. G. Bawendi, *Angew. Chem. Int. Ed.* **2020**, *59*, 860–867.
- [53] P. Cheng, L. Feng, Y. Liu, D. Zheng, Y. Sang, W. Zhao, Y. Yang, S. Yang, D. Wei, G. Wang, K. Han, *Angew. Chem. Int. Ed.* **2020**, *59*, 21414–21418.
- [54] S. Liu, B. Yang, J. Chen, D. Wei, D. Zheng, Q. Kong, W. Deng, K. Han, *Angew. Chem. Int. Ed.* **2020**, *59*, 21925–21929.
- [55] S. Peng, Q. Wei, B. Wang, Z. Zhang, H. Yang, G. Pang, K. Wang, G. Xing, X. Sun, Z. Tang, *Angew. Chem. Int. Ed.* **2020**, *59*, 22156–22162.

RESEARCH ARTICLE

Entry for the Table of Contents



Magic-size clusters (MSCs) have their own unique precursor compounds (PCs). A PC-enabled pathway has been proposed for the transformation from photoluminescent (PL) CdSe displaying one absorption doublet at 373/393 (dMSC-393) to at 433/460 (dMSC-460). This pathway contains three key steps with monomer addition (Step 2) transferring PC-393 to PC-460.